T = total
j = refers to j^{th} microsphere

Superscripts

$-$ = Laplace transformed quantity

LITERATURE CITED

Abramowitz, M., and I. A. Stegun, "Handbook of Mathematical Functions," ed., Dover (1972).

Aifantis, E. C., "A New Interpretation of Diffusion in High Diffusivity Paths—a Continuum Approach," *Acta Metallurgica*, **27**, 683 (1979).

Brenner, H., "The Stokes Resistance of an Arbitrary Particle—Part V. Symbolic Operator Representation of Intrinsic Resistance," *Chem. Eng. Sci.*, **21**, 97 (1966).

Happel, J., and H. Brenner, "Low Reynolds Number Hydrodynamics," Prentice-Hall Inc., 417 (1965).

Hobson, E. W., "The Theory of Spherical and Ellipsoidal Harmonics," Cambridge Univ. Press, 144-63 (1931).

Jury, S. H., "Diffusion in Tabletted Catalysts," *Canad. J. Chem. Eng.*, **55**, 538 (1977).

Layton, L., and G. R. Youngquist, "Sorption of Sulfur Dioxide by Ion Exchange Resins," *Ind. Eng. Chem. Process Des. Develop.*, **8**, 317 (1969).

Lee, L.-K., and D. M. Ruthven, "Kinetics of Adsorption in Bi-Porous Molecular Sieves. Part I: Mathematical Models for Systems with Rectangular Equilibrium Isotherm," *Canad. J. Chem. Eng.*, **57**, 65 (1979).

Lee, L.-K., H. Yucel and D. M. Ruthven, "Kinetics of Adsorption in Bi-Porous Molecular Sieves—Part II: Comparison of Theory and Experiment for Batch Systems," *Canad. J. Chem. Eng.*, **57**, 71 (1979).

Ma, Y. H., and S. Y. Ho, "Diffusion in Synthetic Fanjasite Powder and Pellets," *AIChE J.*, **20**, 279 (1974).

Ma, Y. H., and T. Y. Lee, "Transient Diffusion in Solids with Bipore Distribution," *AIChE J.*, **22**, 147 (1976).

Ruckenstein, E., A. S. Vaidyanathan, and G. R. Youngquist, "Sorption by Solids with Bidisperse Pore Structures," *Chem. Eng. Sci.*, **26**, 1305 (1971).

Tam, C. K. W., "The Drag on a Cloud of Spherical Particles in Low Reynolds Number Flow," *J. Fluid Mech.*, **38**, 537 (1969).

Manuscript received October 22, 1979; revision received February 13, and accepted February 29, 1980.

Fundamental Investigations and Electrochemical Engineering Aspects Concerning an Advanced Concept for Alkaline Water Electrolysis

JUERGEN FISCHER

HANS HOFMANN

GERHARD LUFT

and

HARTMNT WENDT

Institut für Chemische Technologie
Technische Hochschule Darmstadt
Petersenstr. 20, D-610 Darmstadt, FRG

A thorough search for electrocatalysts for anodic oxygen evolution from caustic potash solution together with an investigation for the main reasons of ohmic potential drops in the interelectrode gap has lead to a new concept for an advanced medium temperature (150° to 200°C), medium pressure (30 to 100 bars) alkaline water electrolysis. The new concept will allow electrolytic water decomposition at temperatures between 160° and 200°C with current densities of 1 to 1.5 A/cm² and cell voltages between 1.55 and 1.65 V.

SCOPE

Mixed oxides known to catalyze cathodic oxygen reduction were tested under technical working conditions (current densities 0.5 to 1.5 A/cm², 80° to 260°C, 30 to 60 bars) and judged for their ability to catalyze anodic oxygen evolution from concentrated (30 to 50 wt %) potash solutions in order to reduce cell voltages for electrolytic water decomposition.

The problem of the detrimental gas accumulation which causes waste of electrical energy at gas evolving electrodes was investigated in order to find electrode/diaphragm configurations which minimize or eliminate the voltage drop caused by this bubble curtain effect.

A search for new diaphragms was performed in order to supply a diaphragm for a medium temperature (150° to 250°C) alkaline water electrolysis which would be superior to the classical asbestos diaphragm with respect to corrosion stability and electrical resistance.

Material and corrosion research was performed in order to find an economically attractive construction concept for MT-MP-water electrolyzers.

Correspondence concerning this paper should be addressed to H. Wendt.

CONCLUSIONS AND SIGNIFICANCE

The lanthanum doped perovskite $La_{0.5}Sr_{0.5}CoO_3$ and the spinell type of mixed oxide $NiCo_2O_4$ have proved to be chemically and electrochemically stable and to be good catalysts for anodic oxygen evolution in the temperature range 100° to 200°C.

A sandwich configuration perforated plate cathode/diaphragm/perforated plate anode which allows the gases to be evolved at the electrode backside eliminates largely the effect of gas accumulation observed between electrodes which are spatially separated from the diaphragm.

A new diaphragm is developed which uses a very thin woven nickel net support, the meshes of which are filled and the wires of which are covered by a porous oxide-ceramic material. Such diaphragms exhibit low surface specific electrical resistances (75 $m\Omega cm^2$ if immersed at 30°C in 30 wt % potassium hydroxide). Use of electrode activation together with the new diaphragm concept allows water electrolysis between 160° and 200°C with current densities of 1 to 1.5 A/cm^2 with cell voltages of 1.55 to 1.65 V.

For cell construction, unalloyed steel for the pressure bearing parts with a nickel sleeve of 1 mm thickness protecting the inner parts against surface corrosion and stress corrosion cracking are advised. Projected hydrogen production costs are two to three times as high as the presently valid price for hydrogen production from oil or natural gas.

Present day electrolyzers decompose water electrolytically with nearly 100% current efficiency but with only moderate current densities (0.2 to 0.3 A/cm^2) and with cell voltages which are remarkably higher than the theoretical decomposition potential, namely, 1.8 to 2.2 V. The temperature-dependence of the thermodynamic decomposition voltage is depicted in Figure 1. It increases moderately with the pressure of the evolved gases (30 mV/decade) and decreases slightly with temperature, approximately 80 mV/100°K (see Figure 1). For 20°C and 30 bar, this theoretical decomposition voltage is calculated from the Gibbs free energy for the water splitting reactions (Equations (1*a*), (1*b*), (1*c*) and amounts to 1.254 V (JANAF):

$$H_2O \rightarrow H_2 + \tfrac{1}{2} O_2 \qquad (1a)$$

$$\Delta G^{30\ bars}_{298°K} = +\ 241.94\ KJ/mole$$

$$\Delta H^{30\ bars}_{298°K} = +\ 303.79\ KJ/mole$$

$$E(\Delta G) = \Delta G^{30\ bars}_{298°K}/2F = 1.254\ V \qquad (1b)$$

$$E(\Delta H) = \Delta H^{30\ bars}_{298°K} / 2F = 1.574\ V \qquad (1c)$$

The main reasons for the relatively poor performance of present day water electrolyzers with respect to cell voltage and applied current densities (see Figure 1) (Smith, 1971) are

1. Relatively large overvoltages, especially at the oxygen evolving anode, which are due to expressed kinetic sluggishness of the electrode reactions.

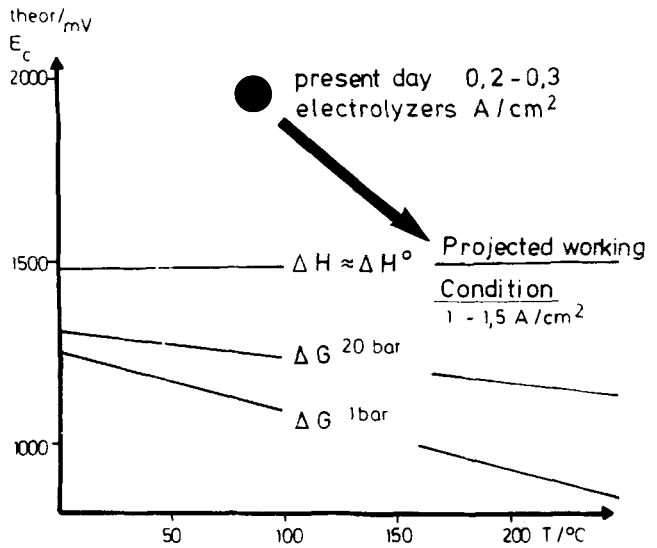

Figure 1. Temperature dependence of theoretical (ΔG) dissociation cell voltage and of enthalpy (ΔH) based cell voltage for electrolytic water decomposition. Demonstration of state of the art of present day electrolyzers and aim of future development.

2. Ohmic voltage drops in the interelectrode gap and within the diaphragm. These diaphragms are fabricated of asbestos cloth. They are mechanically relatively stable but they offer a relatively high surface specific electrical resistance (so-called k value) of 0.3 to 0.4 $\Omega\ cm^2$. In order to avoid excessive and economically unbearable voltage losses in present day electrolyzers, the current densities may not be raised above 0.3 A/cm^2 unless diaphragms with remarkably reduced electrical resistance have been developed.

3. At the upper parts of the vertically arranged electrodes in the used filter press type of electrolyzers, gas bubble accumulation causes reduction of free cross section in the interelectrode gap. Gas bubble accumulation thus leads to an additional increase in ohmic voltage drops, to an increase of effective current densities at the electrode surfaces and hence to an additional increase of overpotential. It is the aim of the work reported in this article to find practical engineering solutions which would allow reduction of ohmic losses and excessive overpotentials in water electrolysis cells to an extent which would permit performance of industrial hydrogen production by water electrolysis with remarkable enhanced current densities of 1 A/cm^2 (or even more) and with nonetheless decreased cell voltages. Both targets aim at a reduction of production price of electrolytically produced hydrogen by reducing investment costs and power costs simultaneously.

CURRENT VOLTAGE MEASUREMENTS FOR ELECTROLYTIC WATER DECOMPOSITION USING DIFFERENT ANODIC ELECTROCATALYSTS AND MECHANICALLY ACTIVATED NICKEL CATHODES IN CAUSTIC POTASH (TEMPERATURE RANGE: 80° TO 260°C)

In 1976 Srinivasan (Miles, 1976) reported on current voltage measurements for electrolytic water decomposition using smooth nickel cathodes (hydrogen evolution) and smooth nickel anodes (oxygen evolution). The temperature range covered by Srinivasan was 80° to 260°C. Srinivasan used the generally applied interruptor technique* to eliminate the ohmic potential drop in the electrolyte between the electrodes. His measurements were repeated in the framework of this investigation for the following reasons:

1. The reproducibility of Srinivasan's measurement was to be tested in order to decide whether the use of unactivated or only mechanically activated (roughened) nickel electrodes together with increased working temperature would allow the cell voltage to decrease for electrolytic water decomposition sufficiently so that the use of any electrocatalyst which might suffer by fouling or deactivation might be avoided.

* The interruptor technique, as explained in the appendix, is used in order to correct measured cell voltages for the ohmic potential drop included in the experimentally obtained cell voltage values.

$$E_{cell} = \phi_{anode} - \phi_{cathode} + I \cdot R_{cell}$$

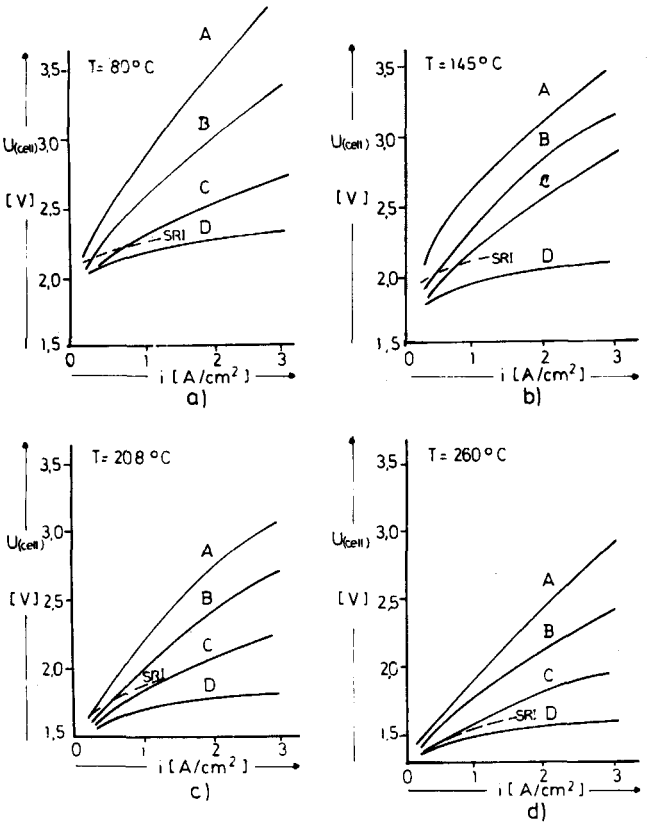

Figure 2*a* to 2*d*. Cell voltage/current density curves at 80°, 145°, 208° and 260°C. Voltages were measured under steady state conditions with 6 mm (A) and 3 mm (B) electrode distance and with the current interrupture method (D). Steady state measurements were extrapolated to zero distance (C). The difference between distance corrected (C) and interruptor corrected current voltage curve (D) is due to the bubble curtain effect. - - - Srinivasan's data (interruptor-corrected). Electrolyte: 50 wt % potassium hydroxide electrodes: sand blasted nickel.

2. It seemed important not only to measure solely (as Srinivasan did) IR voltage drop corrected current voltage curves for electrolytic water decomposition. Instead, the measurements performed should additionally allow us to define and to measure that part of the ohmic voltage drop which is caused by the bubble curtain which develops under stationary and free convection conditions in front of smooth electrodes. A quantitative measurement of this bubble induced voltage drop is of some practical importance in order to find appropriate means to minimize it. In order to separate the bubble induced voltage drop from overvoltage* and ohmic IR potential drops in the interelectrode gap, current voltage correlations for electrolytic water decomposition were determined by two different methods: by the usual current interruptor technique† and by a zero electrode distance extrapolation technique which substracts experimentally the ohmic IR drop from the cell voltage so that the result of this measurement is the difference of the potentials of the working electrodes together with bubble curtain induced voltage drop under the chosen current density. The second method consists of measuring stationary current voltage curves for the nickel cathode/nickel anode assembly by choosing two different electrode distances (namely, 3 and 6 mm). The cell voltages measured for these two electrode distances are then extrapolated to a hypothetical distance of zero.

Figures 2*a* to 2*d* show the zero distance corrected current voltage curves (curves C) for electrolytic water decomposition at smooth nickel electrodes together with the current interruptor corrected values. They are compared with cell voltage current density correlations as obtained experimentally for an electrode distance of 6 mm (curve A) and 3 mm (curve B). Included in Figures 2*a* to 2*d* which represent measurements at four different temperatures are the current interruptor corrected data of Srinivasan's (broken lines). The maximal current densities which are applied in the measurements of Figures 2 are 3 A/cm² and are thus roughly ten times as high as the current densities used in today's technical electrolyzers. The voltage difference between curves C and D approximates the voltage drop due to the bubble curtain induced IR voltage loss and becomes a remarkable fraction of the total cell voltages with current densities of 1 A/cm² and above that value. The most important result of these measurements is, however, that the target (1.5 to 1.7 V cell voltage at 1 to 1.5 A/cm²) may only be achieved without use of any electrocatalyst if the working temperature is raised up to 260°C.

SIMULTANEOUS ELECTROCATALYTIC AND THERMAL ACTIVATION OF ANODIC OXYGEN AND THERMALLY ACTIVATED CATHODIC HYDROGEN EVOLUTION

Mixed oxides which contain cobalt or other transition metals in higher valency states are known to catalyze cathodic oxygen reduction (Tseung, 1978 *a*, *b*). It may be assumed that the same principle may be used, too, to catalyze anodic oxygen evolution (Miles, 1978)

Figure 3 shows current voltage correlations which had been measured at 145°C in 30 wt % potassium hydroxide at parallel, plain nickel electrodes (2 × 2 cm²) and with the same type of electrodes activated by a surface layer of mixed nickel cobalt oxide and of a lanthanum-strontium-cobalt-perovskite ($La_{0.5}Sr_{0.5}CoO_3$), respectively. The surface specific electrocatalyst concentration is already optimized and amounts to 3 to 6 mg mixed oxide/cm².

In all three measurements of Figure 3, the electrode distance amounted to 3 mm, and the measured cell voltages include overvoltages together with the sum of all ohmic potential drops between the two electrodes. The improvement of the cell voltage due to the use of the mixed oxides which catalyze the

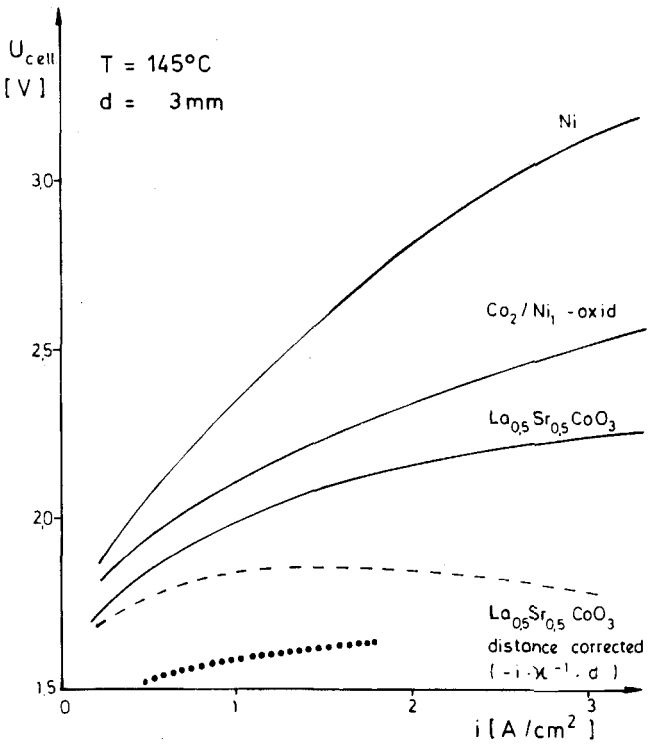

Figure 3. Measured current density cell voltage correlations for smooth, plain nickel electrodes, (electrode distance: 3 mm) with $NiCo_2O_4$ and $La_{0.5}Sr_{0.5}CoO_3$ activated anode. — — distance corrected voltages for LaSrCo-perovskite activated anode. . . . Measured cell voltage for sandwich-configuration and LaSrCo-Perovskite activated anode.

* The overvoltage is the difference of the actual potential from the equilibrium potential of any electrode. For a given rate of electrochemical conversion, that is, for a given current density, this overpotential is higher the more the electrochemical reaction is hindered.

† Current interruptor technique is defined previously and explained in the appendix.

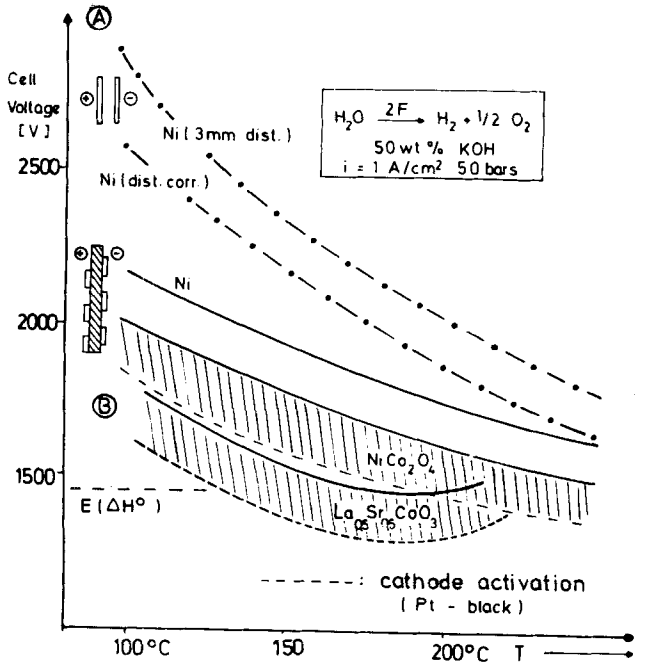

Figure 4. Comparison of cell voltage temperature dependence for electrolytic water decomposition in 50 wt % potassium hydroxide for A: steel blasted nickel electrodes without diaphragm (3 mm), B: optimal anode/diaphragm/cathode configuration and (i) mechanically activated electrodes (ii) $NiCo_2O_4$ activated anode and (iii) $La_{0.5}Sr_{0.5}CoO_3$ activated anode. Data represented by dotted curves are obtained with additional cathode activation by Pt black.

strongly hindered oxygen evolution is so remarkable that one could hope to decompose water electrochemically in technical electrolyzers with current densities of more than 1 A/cm² and with cell voltages of 1.8 V or less at an only moderately enhanced temperature of approximately 175°C. A very important precondition for the utilization of the catalytic effect of mixed oxides is the chemical and electrochemical stability of the used electrocatalysts. Indeed, although the electrocatalysts nickel cobalt mixed oxide and lanthanum-strontium-cobalt-perovskite seem to be very sensitive against passive corrosion (they decompose on nickel anodes being immersed in aqueous caustic potash without any definite anodic polarization), and although these mixed oxides quickly deteriorate upon cathodic polarization, they seem to be sufficiently stable under anodic polarization conditions. Both mixed oxides show no loss of their electrocatalytic activity on continuous operation over up to 1 000 hr at 1 A/cm² at temperatures between 120° and 200°C. Upon repeatedly interrupted use, an accumulated working time under these working conditions was already obtained which amounted to more than 2 600 h. (After that time, several anodes were destroyed by accidental short circuiting and a reversed polarization of the electrolysis cell.)

Figure 4 shows the influence of temperature on electrocatalyzed anodic oxygen and cathodic hydrogen evolution. In Figure 4, the measured current density cell voltages for a current density of 1 A/cm² are plotted vs. temperature. Cell voltages were measured for an optimized cell configuration which eliminates the detrimental bubble accumulation to a remarkable degree. Measured cell voltages include, however, ohmic potential drops between the electrodes which are determined mainly by the specific electrical resistivity of the electrolyte [($\Delta U_\Omega \propto \rho$(electrolyte)]. Additionally, Figure 4 includes some information on electrocatalysis of cathodic hydrogen evolution. The broken lines represent measured cell voltages where platinum black (2 mg/cm²) had been applied to the cathodes as the most effective electrocatalyst known. Although platinum black is too expensive an electrocatalyst which may not be used in commercial electrolyzers, its application may serve to gain some information on potential gain in cell voltage by use of any potent cathodic electrocatalyst. Except platinum and platinum metals as cathodic electrocatalysts, only the application of sinter nickel [enhancement of true surface over the geometrical electrode surface Nayar (1978)] and doped sinter nickel (Appleby, 1978) seems to be of some value to activate nickel cathodes which are to be used at enhanced temperatures and enhanced current densities. The usual sulfide activation is relatively inefficient, and nickel sulfide is thermodynamically unstable under practical electrolysis condition. Whatever the final choice for electrolysis of cathodic hydrogen evolution will be, it may be concluded from Figure 4 that an additional improvement of cell voltage by 100 to 150 mV at 1 A/cm² may be obtained.

PARTIAL ELIMINATION OF THE DETRIMENTAL BUBBLE ACCUMULATION BY USING PERFORATED PLATE ELECTRODES AND A SANDWICH CONFIGURATION OF PERFORATED PLATE ELECTRODES PRESSED ON BOTH SIDES OF THE DIAPHRAGM

Conventional water electrolyzers use an electrode diaphragm configuration with a narrow gap of 1 to 2 mm between the flat electrode and the diaphragm surface (see Figure 5*a*). This configuration implies that ascending from bottom to top of the electrolyzer, the volume ratio of gas to electrolyte increases steadily. The consequences are twofold. First, the effective specific electrical resistance of the electrolyte decreases. According to Tobias (1959) and Mashovets (1951), an approximate empirical correlation, Equation (2), predicts that at a volume ratio of gas/electrolyte 1/3 (i.e. $\epsilon_{gas} = 25\%$), the specific resistance ρ

$$\rho(\epsilon)/\rho_0 = (1 - \epsilon)^{-1.5} \text{ (Tobias, 1959)} \qquad (2a)$$

$$\rho(\epsilon)/\rho_0 = (1 - 1.78\epsilon + \epsilon^2)^{-1} \text{ (Mashovets, 1951)} \qquad (2b)$$

increases by a factor of 1.6 to 1.7. Second, owing to partial coverage of the electrode surfaces by gas bubbles, the effective current density increases. According to the Butler-Volmer equation which describes the current density vs. electrode potential correlation of any electrode process, a 50% coverage of the electrode surface would demand an increase in overpotential by some 40 mV, so that a mean bubble coverage

$$i = i_0 \cdot \exp\{\pm \alpha \cdot F \cdot \Delta\rho/RT\}$$

$$+ \text{ for anodic, } - \text{ for cathodic processes} \qquad (3)$$

of both electrodes of 50% would result in approximately 100 mV total increase in overvoltage.

A tightly sandwiched configuration of perforated electrodes which are pressed to both sides of the diaphragm (see Figure 5*b*) is expected to eliminate the gas-bubble accumulation effect at least partly. The broken line in Figure 3 demonstrates the gas bubble effect as it is observed at small (2 × 2 cm²) plain, smooth

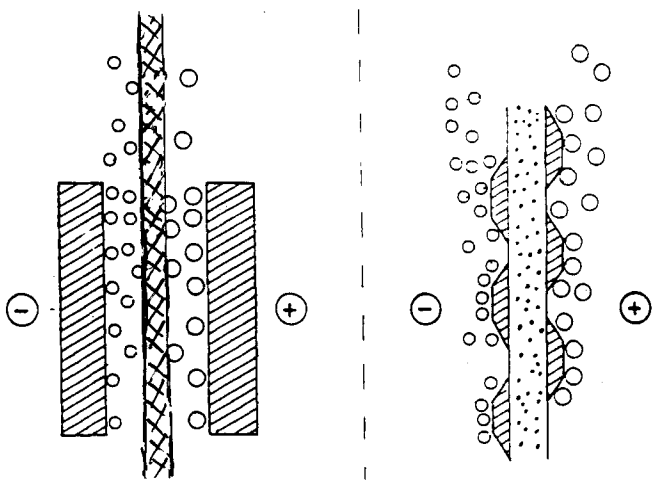

Figure 5. *a*. Conventional electrolyzer configuration for gas evolving electrodes *b*. Sandwiched configuration for gas evolving electrodes: perforated plate electrodes pressed to either side of the electrolyzer.

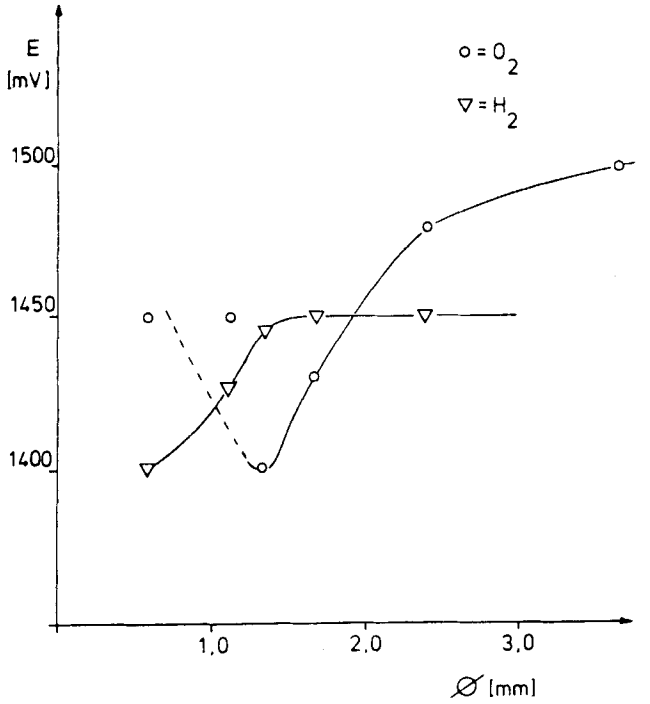

Figure 6. Experimental determination of optimal diameter of openings for perforated plate anode (O_2) and cathode (H_2), respectively.

electrodes. The broken line is obtained by subtraction of the calculated ohmic voltage drop:

$$\Delta U_\Omega = i \cdot \kappa^{-1} \cdot d \tag{4}$$

The appearance of a voltage maximum at approximately 1 A/cm^2 for the electrolyte resistance corrected current density/cell voltage correlation is explained by the fact that at higher current densities gas evolution causes strong bubble bouyancy induced natural convection which very effectively removes the gas bubbles from the electrode surface. At lower current densities, diffusion of oxygen away from the electrode very likely reduces the number of bubbles accumulating and sticking to the electrode.

If the electrode/diaphragm/electrode configuration is changed from a to b (in Figure 5), the measured cell voltages are remarkably decreased, especially at the critical current density range around 1 A/cm^2. A precondition for this improvement, however, is appropriate matching of the electrode openings to the mean bubble diameter of the evolved gases which is different for hydrogen (20 to 30μm) and oxygen (0.5 mm) (Sillen, 1978). A simple calculation shows that opening dimension and dimensions of particulate electrode parts should be as small as possible in order to make efficient use of the back side of an electrode for gas evolution. However, too small openings will cause bubble trapping.

Figure 6 demonstrates the experimentally applied method which was used to match cathode and anode openings to the demand that bubble trapping in the openings must be avoided. Cell voltages are measured for a standardized current density of 1 A/cm^2 in relation to the opening diameters of perforated plate anodes and cathodes, respectively, with geometry and opening diameter of the respective counter electrode being kept constant. Figure 6 demonstrates that below an opening diameter of 1.2 mm, oxygen bubbles become trapped so that for smaller openings, total cell voltages increase again. For hydrogen, the optimal opening diameter is smaller than 0.3 mm but certainly above 0.1 mm. For practical reasons (mechanical stability and handling of perforated electrodes), the opening diameter for cathodes can be chosen arbitrarily between these limits, whereas the optimal opening diameter of 1.2 mm for the anodes should be strictly maintained.

TABLE 1. NECESSARY CHARACTERISTICS OF A DIAPHRAGM TO BE USED IN ELECTROLYZERS WITH GAS EVOLVING ELECTRODES

Surfaces spec. electr. resistance [Ω cm^2]	Max. surface spec. hydrodyn. permeability [cm^3 centipoise/cm^2 · bar · s]	Pore diameter [cm]
$<7.10^{-2}$	>5	$(1 \div 10)\ 10^{-4}$

DEVELOPMENT OF A NEW DIAPHRAGM CONCEPT

The purpose of the diaphragm in an electrolysis cell which produces gases at either electrodes is threefold:

1. The diaphragm has to prevent unhindered intermixing of catholyte and anolyte. The gas evolution at both electrodes forms a two phase mixture of electrolyte with more or less dispersed bubbles so that intermixing of anolyte and catholyte always means intermixing of the two gases which should be prevented strictly in order to obtain high gas purities and current efficiencies, respectively.
2. The diaphragm must form an efficient diffusion barrier for the gas molecules in order to prevent contamination of the evolved gases by molecular diffusion of the gas evolved at the respective counter electrode.
3. The diaphragm may be used to prevent very efficiently the formation of a gas bubble curtain at the front side of the electrodes just by pressing the electrodes onto the more or less elastic diaphragm. Most important is that clogging of the diaphragm pores by gas bubbles which may either intrude into the pore mouths or which may precipitate out within the pores from supersaturated electrolyte solutions must be excluded completely lest the electrical resistance of the diaphragm increases in an uncontrolled manner. Bubble formation in small cavities, pores, etc., of radius r may only be observed if a certain degree of supersaturation is established:

$$p - p_{sat} \leq \frac{2\sigma}{r} \tag{5}$$

Owing to gas evolution at the back side of the electrodes, the supersaturation of the gas in the electrolyte which contacts or diffuses or drifts into the diaphragm pores will be largely reduced (compared to the supersaturation at the electrode back side). Under a working pressure of 30 to 60 bars, supersaturation pressures of hydrogen and oxygen of no more than a few bars will exist at the diaphragm surface. According to Equation (5) for $\sigma \approx 200$ dyn/cm, pore diameters of some micrometers will prohibit gas clogging of the diaphragm reliably.

Anolyte and catholyte are saturated with oxygen and hydrogen, respectively. Therefore, the diaphragm has not only to keep the gases apart from each other but must additionally offer

Figure 7. Enlarged view of surface of oxide-ceramic covered metal screen.

TABLE 2. CHARACTERISTIC DATA OF OXIDE-CERAMIC COVERED NICKEL SCREEN DIAPHRAGMS AND THEIR COMPARISON WITH COMMERCIALLY AVAILABLE MATERIAL (3., 4., 5.)

Composition of oxidic mixture	Surface spec. electr. resistance (immersed in 30wt%KOH) [Ω cm^2] meas. at 30°C	Surface spec. hydrodyn. permeability $\left[\frac{\text{cm}^3 \cdot \text{centipoise}}{\text{cm}^2 \cdot \text{bar} \cdot \text{s}}\right]$	Mean pore diam. [μm]	Corrosion rate g/m^2/d
1. 50% $K_2Ti_6O_{13}$ 50% NiO	0.075	0.4	2-3	0.25
2. 45% $BaTiO_3$ 45% ZrO_2 5% $K_2Ti_6O_{13}$ 5% Na_2Co_3	0.027	1	1	0.04
3. Porous ZrO_2-plate	0.260	200	30-40	0.46
4. ZrO_2-cloth	0.032	103	100	1.00
5. Nafion® (K^+-loaded)	10.60	0	—	—

a sufficiently high hydrodynamic resistance to retard intermixing of oxygen saturated anolyte with hydrogen saturated catholyte due to occasional pressure differences between cathode and anode chambers.

If a contamination of less than 1% of the gases will be allowed, then Equations (6*a*) and (6*b*) determine the relative magnitude of hydrogen and oxygen cross flow flux densities ($\dot{n}$) and production densities*:

$$(\dot{n}^{O2}) \text{ cross flow} < 10^{-2}(\dot{n}^{H2}) \text{ production} \qquad (6a)$$

$$(\dot{n}^{H2}) \text{ cross flow} < 10^{-2}(\dot{n}^{O2}) \text{ production} \qquad (6b)$$

Cross flow fluxes of the gases are determined by volumetric flow rate of the electrolyte and the saturation concentration of the respective gas Equation (7*a*). The volumetric flux density $\dot{v}$[cm^3/cm^{2}s] across the membrane depends on the applied pressure difference Δp, the viscosity of the electrolyte η and the surface specific hydrodynamic permeability κ_{hydro}:

$$(\dot{n}^{\text{gas}})_{\text{cross flow}} = \dot{v}_{\text{electrolyte}} \cdot c_s^{\text{gas}} \qquad (7a)$$

$$\dot{v} \cdot c_s^{O2} = \kappa_{\text{hydro}} \cdot \Delta p \cdot c_s^{O2} < 0.5 \cdot 10^{-2} \cdot i/F \qquad (7b)$$

$$\dot{v} \cdot c_s^{H2} = \kappa_{\text{hydro}} \cdot \Delta p \cdot c_s^{H2} < 0.25 \cdot 10^{-2} \cdot i/F \qquad (7c)$$

The saturation concentration of hydrogen in concentrated caustic potash in the temperature range which is of special interest for alkaline water electrolysis is well known (Vogel et al., 1967). It does not exceed some 10^{-3} mole/l under 30 to 60 bars hydrogen pressure. For oxygen, these data are less well known but can be estimated to be larger than for hydrogen (Knaster, 1964; Vogel, 1968). But, certainly, the oxygen solubility will not exceed that of hydrogen by more than a factor of 10. So with an assumed saturation concentration of 10^{-2} mole/l for oxygen in 30 to 50% caustic potash and a driving pressure difference of 10^{-3} bars (which certainly are the highest possible hydrostatic pressure fluctuations in the electrolyzer), and using a minimal viscosity for the electrolyte of 1 centipoise (Vogel et al., 1967), one calculates [Equation (7*a*)] a maximal surface specific hydrodynamic permeability of the diaphragm of

$$\kappa_{\text{hydro}}^{\max} \approx 5[\text{cm}^3 \cdot \text{centipoise/cm}^2 \cdot \text{bar} \cdot \text{s}] \qquad (7d)$$

Although according to this estimation a relatively high surface specific hydrodynamic resistance of the diaphragm is necessary, it nevertheless must offer only a low electrical surface specific resistance if immersed in the electrolyte. The surface specific electrical resistance must not exceed 0,1Ωcm^2 and should rather be around 30 to 50 mΩcm^2 in order to avoid too high ohmic potential drops within the diaphragm at applied current densities around 1 A/cm^2. Table 1 collects the different conditions which should be allowed for by a diaphragm which should be used in an electrolysis process with gas evolving electrode reactions being run at current densities around and above 1 A/cm^2.

Because of the thermodynamic instability of asbestos (chrysotile) in caustic potash (Gras, 1978), it seems necessary to develope a completely new diaphragm material which is based on a porous refractory structure. This material due to its chemical composition should be more stable against caustic corrosion than asbestos. It should be supported by a metallic screen or net structure in order to provide the whole compound structure with the necessary mechanical strength and flexibility in spite of the brittleness of the oxide-ceramic material. The fact that the supporting metallic net is covered by the oxide-ceramic material provides the necessary electrical insulation (Hofmann and Wendt, 1978). Such structures are easily obtained by covering woven metal nets of very fine size (0,3 mm wire diameter, 0,52 mm mesh width) by conventional techniques with an aqueous slurry of finely ground grains of the respective oxide-ceramic material. After the slurry cover is carefully dried, it is sintered at appropriate temperatures. Figure 7 shows the surface of such oxide-ceramic covered metal screen diaphragm, the porosity of which can be carefully adjusted in order to supply the necessary high hydrodynamic resistivity with the necessary low electrical surface specific resistance. Such structures can be produced with a total thickness of no more than 300 to 400 μm, and they can be bent with a bending diameter of 15 cm without being broken or showing cracks or fissures of the oxide-ceramic cover.

Table 2 gathers the relevant physical characteristics of two such oxide-ceramic covered nickel net diaphragms and compares them with the respective data of commercially available zirconia porous sinter, zirconia cloth and a Nafion® membrane. The data of Table 2 clearly show that the newly developed diaphragm version does fulfill nearly all demands, and only its corrosion stability is to be improved still further.

It should be stressed that long time performance tests of optimized metal net support porous oxide-ceramic materials prove excellent stability of this important electrolyzer component over more than 6 000 hr accumulated. Therefore, the cell voltage data given in Figures 2 and 3*b*, respectively, with lanthanum-strontium-cobalt-perovskite activated anodes which have been measured with the use of porous oxide-ceramic diaphragms may be assumed to be reliable data. They, indeed, could be reproduced many times with independently produced cell components.

CONSTRUCTION MATERIALS FOR AN ADVANCED ALKALINE WATER ELECTROLYZER WORKING AROUND AND ABOVE 150°C

Metallic Materials for Cell Frames, Tubings and Gas-Liquid Separators

In choosing the appropriate construction material for the pressure bearing parts of an electrolyzer, one has to account for the fact that surface corrosion as well as stress corrosion cracking becomes markedly enhanced if the working temperature of electrolyzers working with alkaline electrolytes is raised above 100°C. This is the reason why cheap austenitic steels can be used for the pressure bearing parts only if direct contact of hot al-

* In Equations (6*a*) and (6*b*), flux densities are used instead of total fluxes in order to be able to express gas production rates by current densities.

TABLE 3. POLYMERIC MATERIAL AND TEMPERATURE LIMIT FOR THEIR USE

Material	a* 5 deg below creeping point	b† Highest temperature if used in contact with conc. KOH
1 Polyfluoroethylene-propylene	205°C	120°C
2 Polyarylether-sulfone	260°C	120°C
3 Poly-perfluoroakyl-vinyl-ether	260°C	200°C
4 Poly-tetrafluoro-ethylene	260°C	220°C
5 Polyphenylene-sulfide (Ryton R6®)	260°C	230°C

* See: Werkstoff-Führer Kunststoffe.
† 1 through 5: own results.

TABLE 4.

Electrolyzer	Lurgi	Filter press electrolyzer of the Lurgi type equipped with advanced components and improved configuration Version 1*	Version 2†	Version 3**
U_{cell}[V]	1,9	2,0	1,65	1,80
Current density [A/cm²]	0,2-0,3	1,0	1,0	1,5
Working temp. [°C]	90	90	170	170
Working press [bar]	30	30	60	60
Capital costs [US \$/N m³ H_2]	0,0827	0,0497	0,0620	0,04152
Energy costs [US \$/N m³ H_2]	0,1372	0,1428	0,1181	0,1287
Maintenance [US \$/N m³ H_2]	0,0140	0,0140	0,0140	0,0140
Total price [US \$/N m³ H_2]	0,234	0,212	0,194	0,1842

* Conventional steel construction, c.d.: 1 A/cm².
† Steel construction covered internally by 1 mm nickel sleeves c.d.: 1 A/cm².
** Version 3 identical with version 2 c.d.: 1,5 A/cm² energy price: 0,026 US \$/kWh; utility: 100%; depreciation time: 5 yr.

kaline electrolyte and steel is prevented. On the other hand, steels may be substituted by suitable alloys which possess a very high nickel content and owing to this circumstance are much more resistant against caustic corrosion than unalloyed steels. However, the use of steels or other alloys with very high nickel content (hastelloy, inconel and monel) is prohibitive owing to the relatively high costs and limited corrosion stability of these materials. Low carbon-nickel is the only metal known, which, except for the much too expensive zirconium or silver, possesses nearly perfect stability against alkaline corrosion under the temperature and concentration of an advanced alkaline water electrolysis. Low carbon-nickel, however, is too weak as construction material and furthermore much too expensive to be used in compact form to construct the metallic components of an electrolyzer. It is, therefore, possible to choose as a compromise between the demand for high surface corrosion resistance and high tensile strength and low cost a compound structure in which the pressure bearing parts of the electrolyzer and auxiliary equipment are constructed of normal steel but which are protected in their interior by nickel sleeves of sufficient thickness.

Nonmetallic Materials for Electrically Insulating Gaskets

A detailed corrosion test program was performed in order to find a suitable, cheap, easy to process nonmetallic material which could serve for the fabrication of gaskets and other electrically insulating components of the electrolyzer. The materials for these components have to be resistant against caustic corrosion to such an extent that they can stay practically indefinitely in contact with hot (150° to 250°C) concentrated (30 to 50 wt % potassium hydroxide) caustic potash without being dissolved by chemical decomposition and without a remarkable change in their physical characteristics. Table 3 gathers the limiting temperature and potassium hydroxide concentration range for four different extraordinary stable polymers. Below these limits the respective polymer can be assumed to possess the necessary corrosion resistance and thermal stability to serve for long lasting use in alkaline water electrolyzers. It is quite clear that only PTFE and Ryton^R may be used for the most enhanced temperatures and potassium hydroxide concentrations. The data of Table 3 show that an advanced water electrolysis should be run at working temperatures well below 260°C and that for Ryton^R and PTFE, a working temperature of not higher than 200°C should be envisaged owing to the limited chemical and thermal stability of the polymeric materials which are to be used for the electrically insulating nonmetallic electrolyzer components.

COMPLETE CONCEPT OF AN ADVANCED WATER ELECTROLYZER AND PRELIMINARY ESTIMATION OF HYDROGEN PRODUCTION COSTS

Based on the cell voltage temperature dependence as measured with an optimized sandwich arrangement of perforated plate anode/oxide-ceramic diaphragm/perforated plate cathode, a maximum working temperature of + 200°C with a 50 wt % potassium hydroxide is chosen. The high vapor pressure (4 to 5 bars) for these temperatures necessitates a working pressure of 50 to 60 bars. The electrolyzer is constructed according to the filter press concept and uses the well-known arrangement of bipolar nickel electrode (0.5 mm thick) with the perforated Vor-Elektrode (Lurgi-electrolyzer) being pressed from either side onto the diaphragm.

Cell frames, tubes and gas/liquid separation vessels are fabricated of normal unalloyed steel and are all equipped at their inner walls with a low carbon-nickel sleeve of 1 mm thickness. If a maximum working pressure of 100 bars (intended to be used are only 60 bars) and outer diameter of 750 mm is chosen, then a thickness of the steel ring of 3 cm is required. For an electrolyzer which produces 750 Nm^3hydrogen/h with a current density of 1 A/cm² and a cell voltage of 1.6 V, the costs for the total equipment and the hydrogen production as given in Table 4 are estimated. Assumed power costs amount to 0.025 US \$/kWh, and an annual depreciation of 20% together with 8% interest are taken into account.

DISCUSSION

The preliminary cost estimation given in Table 4 does not compare very favorably with the costs for hydrogen production from oil or natural gas which amounts to approximately 0.08 US \$/Nm^3H_2. Nevertheless, the estimated costs which make use of all the available improvements are shown to be remarkably lower than the production cost of a conventional high pressure electrolyzer.

The electrode kinetic data which had been reported by Grimes and Costa (Grimes, 1967) more than 10 yr ago (1.8 V cell voltage at 120°C and 1 A/cm² c.d.) are largely outdated, and cell voltages are now near or even actually below the so-called thermoneutral value, so that the vaporization enthalpy for the steam which is contained in the steam saturated hydrogen and oxygen product gases already has to be supplied by the introduction of additional process heat. But still further improvement in

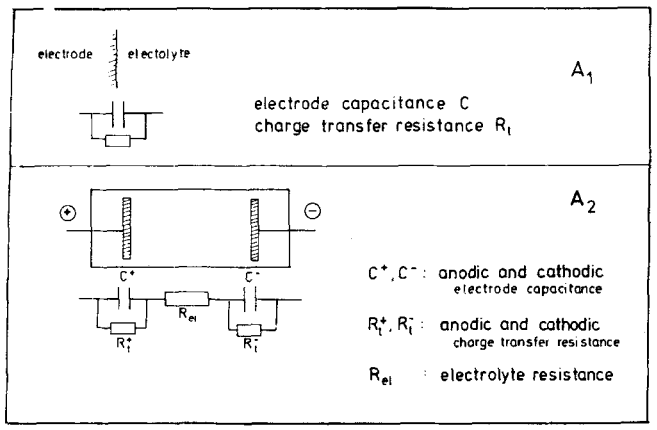

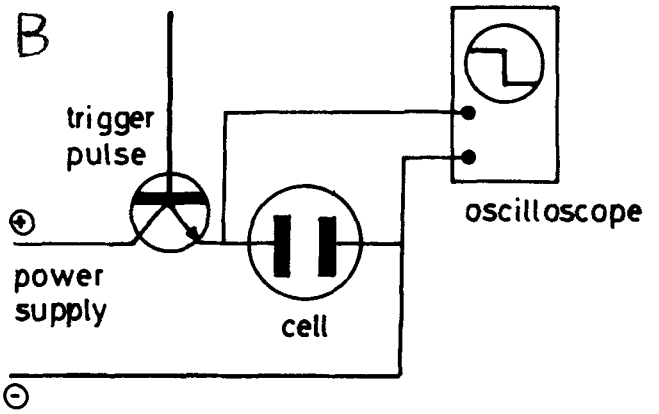

Figure A1. A: Impedance model of single electrode and electrolysis cell. B: Electronic switching device to measure current interruptor corrected cell voltages.

the anodic activation may not be excluded so that even some fraction of the entropic part of the process enthalpy ($T\Delta S$) may be supplied in the future by process heat at temperatures between 150° and 200°C. There is ample access to this, best at the low temperature low pressure outlet of thermal power plants based on nuclear, solar or geothermal sources.

EXPERIMENTAL

Electrode kinetic measurements as well as measurements of cell voltages in complete, sandwiched electrode/diaphragm/electrode stacks were performed with 1×1 cm^2 and 2×2 cm^2 electrode and diaphragm samples in a stainless steel autoclave of 200 cm^3 inner volume. Internal pressure within the pressure range 30 to 100 bars was maintained by compressed nitrogen, and internally produced hydrogen and oxygen were recombined in the autoclave by catalytic combustion at a platinum catalyst deposited on charcoal.

All measurements were extended over several hundred hours. Corrosion tests were performed by contacting samples of the respective material (0.1 to 0.5 g) with caustic potash in small stainless steel autoclaves (20 cm) which were covered in their interior by a 1 mm thick nickel sleeve. After exposure for different times, samples were examined gravimetrically and by microscopic inspection.

ACKNOWLEDGMENT

The authors performed this work in the frame of an R and D contract of the European Community (047-76 EHD). They gratefully acknowledge the financial support of the Community and the fruitful and stimulating atmosphere among all contractors of the ECC-water electrolysis program. The authors acknowledge additional support of the "Fonds der Chemie" which supplied many of the routine equipment being used for this investigation.

APPENDIX: CURRENT INTERRUPTOR CORRECTED MEASUREMENT OF CELL VOLTAGES

As shown in Figure A1, the impedance of an electrolysis cell is mainly given by the two-electrode impedances (modeled by the electrolyte/electrode capacitance and the charge transfer resistance in parallel) and the electrolyte resistance in between. Upon a virtually instantaneous current interruption, as it may be performed by an appropriate semiconductor device, the ohmic potential drop across the electrolyte resistance decays instantaneously to zero. This is not the case for the potential differences across the electrode impedances because of the electronic charge which is accumulated in the electrochemical double layer which is modeled as the electrode capacitance. At the very beginning of the electrode potential decay, immediately after switching off the cell current, the change of electrode potential with time may be linearized, as given

$$dU/dt = i/C(\text{electrode}) \qquad \text{(A1)}$$

With $C(\text{electrode}) \approx 20 - 30\ \mu F\ \text{cm}^{-2}$ and $i = 1$ A/cm^2, one obtains for the rate of potential change 5.10^4 V/s. This means that in order to commit no mistakes in potential measurements greater than 20 mV, the cell current has to be switched off faster than 4.10^{-7} s. Such short switching times are possible, indeed (Lorenz, 1954; Piontelli, 1954).

NOTATION

c^i = concentration of species i
c_s^i = saturation concentration of species i
C (electrode) = electrode capacitance
d = electrode distance
F = 1 Faraday = 96 500 As
ΔG = reaction free enthalpy
ΔH = reaction enthalpy
I = current
i = current density
i_0 = exchange current density
$\dot{n}$ = molar flux density
p = pressure
R = electrical Resistance
R = gas constant
r = radius of pores
T = temperature
t = time
U = voltage
ΔU_Ω = Ohmic potential drop
$\dot{V}$ = surface specific volumetric flux rate

Greek Letters

α = charge transfer coefficient ($\approx 0{,}5$)
ϵ = void fraction
ϕ = electrical potential
$\Delta\phi$ = overpotential = $\phi - \phi$ (equilibrium)
κ = specific electrical conductivity
κ_{hydro} = surface specific hydrodynamic permeability
η = viscosity
ρ = specific electrical resistance
σ = surface tension

LITERATURE CITED

Appleby, A. J., and G. Crepy, "Improvements in Electrolysis Technology in Alkaline Solutions," *Proc. of the 2nd World Hydrogen Energy Conference*, Zürich, 1978, Vol. 1, p. 227.

Costa, R. L., and P. G. Grimes, "Electrolysis as a Source of Hydrogen and Oxygen," *Chem. Eng. Progr. Symposium Ser.*, **63**, 45 (1967).

Gras, J. M., and J. J. le Coz, "Asbestos Corrosion Studies," in *Hydrogen Energy Systems*, Proc. of the 2nd World Hydrogen Energy Conference, Zürich, 1978, Vol. 1, p. 255.

Hofmann, H., and H. Wendt, "Korrosionsstabile Diaphragmen und Filter mit Oxidkeramik-Beschichtung, P/1919, Lu 1515, 10. 4. (1978).

JANAF, Thermochemical Tables, 2 ed., NSRDS-N BS 37 (1971).

Knaster, M. B., and L. A. Appelbaum, "Solubility of Hydrogen and Oxygen in Concentrated Potassium Hydroxide Solutions," *Zh. Fiz. Khim*, 38, 223 (1964).

Lorenz, W., "Oszillographische Überspannungsmessungen I," *Zeitschrift f. Elektrochemie*, **58**, 10 (1954).
Mashovets, V. P., "The Effect of Non Conducting Inclusions on the Conductivity of an Electrolyte," *Zh. Prikladn. Khim.*, **24**, 391 (1951).
Kissel, G., P. W. T. Lu, M. H. Miles and S. Srinivasan, "Hydrogen Production by Water Electrolysis," *Rec. Intersc. Energy Conversion Eng. Conf.*, p. 1194, New York (1975).
Miles, M. H., G. Kissel, P. W. T. Lu and S. Srinivasan, "Effect of Temperature on Electrode Kinetic Parameters for Alkaline Hydrogen and Oxygen Evolution Reactions on Nickel Electrodes in Alkaline Solutions," *J. Electrochem. Soc.*, **123**, 332 (1976).
Miles, M. Y., Y. H. Huang and S. Srinivasan, "The Oxygen Electrode Reaction in Alkaline Solutions on Oxide Electrodes Prepared by the Thermal Decomposition Method," *ibid.*, **125**, 193 (1978).
Nayar, M. G., P. Ragunathan and S. K. Mitra, "Development and Operation of a High Current Density, High Pressure Advanced Electrolysis Cell," in *Hydrogen Energy Systems*, Proc. of the Second World Hydrogen Energy Conference, Zürich, 1978, Vol. 1, p. 451.
Piontelli, R., U. Bertocci, G. Bianchi, G. Ginerei and G. Poli, "Meßmethoden der Polarisationsspannungsmessungen," *Zeitschrift f. Elektrochemie*, **58**, 2 (1954).
Sillen, C. W. M. P., "Gas Bubble Formation During Water Electrolysis," in *Seminar on Hydrogen as an Energy Vector, its Production, Use and Transportation*," Brussels 3 and 4 Oct. 1978; Ed: Comm. of the Europ. Comm., EWR 6085 DE/EN/FR/IT (1978).
Smith, D. E., "Industrial Water Electrolysis," in *Industrial Electrochemical Processes*, A. Kuhn, ed., Elsevier (1971).
Tseung, A. C. C., and K. L. J. Yeung, "Reduction of Oxygen on Teflon-bonded Ni Co_2 O_4/Graphite Electrodes," *J. Electrochem. Soc.*, 125, 1003 (1978).
Tseung, A. C. C., "Semiconducting Oxide Oxygen Electrodes," *ibid.*, 1660 (1978).
Tobias, C. W., "Effect of Gas Evolution on Current Distribution and Ohmic Resistance in Electrolysis," *ibid.*, **106**, 833 (1959).
Vogel, W. M., K. J. Routsis, V. J. Kehrer, D. A. Landsmann and J. G. Tschinkel, "Some Physicochemical Properties of the KOH-H_2O-System," *J. Chem. Eng. Data*, **12**, No. 4, 467 (1967).
Vogel, W. M., and S. W. Smith, "An Electrochemical Method for the Determination of the Solubilities of a Reaction Gas in an Electrolyte," *J. Electroahal. Chem.*, **18**, 215 (1968).
Wekstoffführer Kunststoffe, Carl Hanser Verlag, München, Wien (1975).

Manuscript received April 10, 1979; revision received February 12, and accepted February 29, 1980.

Dynamics of Mixed Cultures of Microorganisms: Some Topological Considerations

Structural relationships between the numbers of the various types of steady states exhibited by a mixed culture of microorganisms growing in a chemostat have been obtained. The analysis is based on the degree theory and utilizes Hopf's index theorem. Useful information concerning the culture growth and general conclusions pertaining to the nature of the possible steady states are obtained from these relationships. An alternate method of stability analysis, based on the above results, has also been developed and applications to several cases of growth of indirectly interacting populations which demonstrate the efficiency of the method are presented.

GREGORY STEPHANOPOULOS

Department of Chemical Engineering
California Institute of Technology
Pasadena, California 91125

SCOPE

A continuous flow biochemical reactor in which a mixed culture of microorganisms is growing very often exhibits multiple steady states. The analysis of the stability of these steady states has been the subject of many works so far. Invariably, these analyses have been based on Liapounov's first method, and in many cases they have produced very informative results concerning the dynamic behavior of interacting microbial populations. There are indirect interactions, however, where analytical solutions for the steady states cannot be obtained, and the stability of a steady state is determined by numerical evaluation of the steady states and, subsequently, the eigenvalues of the linearized system. One disadvantage of this approach is the limited generality of the so obtained results. Taylor and Williams (1974), for example, examined the growth in a chemostat of a culture consisting of two populations growing on two rate limiting substrates for which they competed. Among other possibilities, they also investigated the case of two coexistence steady states, and although their numerical calculations indicated that these steady states were never meaningful and stable at the same time, this result could not be shown in general through the linearized stability analysis.

Similar problems arise in the analysis of other types of indirect interactions, especially when the number of the environmental variables affecting the growth rates of the two populations becomes large. The objective of this work, then, has been to develop some means of facilitating the stability analysis and obtaining general results on the nature of the various steady states which are possible in such systems. This is accomplished through the development of some topological relationships between the numbers of the various types of steady states exhibited by a mixed culture of microorganisms growing in a chemostat. These relationships utilize the results of the degree theory and Hopf's index theorem and recognize some general mathematical laws governing the structure of the differential equations which describe the dynamics of growth of the mixed culture. The importance of these relationships lies in the ease with which one determines the type and therefore the stability of a steady state from relatively limited information and in the generality of the obtained results.